

This is the accepted manuscript made available via CHORUS. The article has been published as:

## Discovering new gauge bosons of electroweak symmetry breaking at LHC-8

Chun Du, Hong-Jian He, Yu-Ping Kuang, Bin Zhang, Neil D. Christensen, R. Sekhar Chivukula, and Elizabeth H. Simmons

Phys. Rev. D **86**, 095011 — Published 8 November 2012

DOI: [10.1103/PhysRevD.86.095011](https://doi.org/10.1103/PhysRevD.86.095011)

# Discovering New Gauge Bosons of Electroweak Symmetry Breaking at LHC-8

Chun Du<sup>1</sup>, Hong-Jian He<sup>1,2</sup>, Yu-Ping Kuang<sup>1</sup>, Bin Zhang<sup>1</sup>

<sup>1</sup> *Center for High Energy Physics, Tsinghua University, Beijing 100084, China*

<sup>2</sup> *Theory Division, CERN, CH-1211 Geneva 23, Switzerland*

Neil D. Christensen

*Pittsburgh Particle Physics, Astrophysics and Cosmology Center,*

*Department of Physics and Astronomy, University of Pittsburgh, Pittsburgh, PA 15260, USA*

R. Sekhar Chivukula, Elizabeth H. Simmons

*Department of Physics and Astronomy, Michigan State University, East Lansing, Michigan 48824, USA*

We study the physics potential of the 8 TeV LHC (LHC-8) to discover, during its 2012 run, a large class of extended gauge models or extra dimensional models whose low energy behavior is well represented by an  $SU(2)^2 \otimes U(1)$  gauge structure. We analyze this class of models and find that with a combined integrated luminosity of  $40 - 60 \text{ fb}^{-1}$  at the LHC-8, the first new Kaluza-Klein mode of the  $W$  gauge boson can be discovered up to a mass of about  $370 - 400 \text{ GeV}$ , when produced in association with a  $Z$  boson.

PACS numbers: 12.60.Cn, 11.10.Kk, 12.15.Ji, 13.85.Qk

[arXiv:1206.6022]

Preprint#: CERN-PH-TH/2012-177, MSUHEP-120618, PITT-PACC-1206, TUHEP-TH-12177

## I. 1. INTRODUCTION

By the end of 2011 the LHC, running at a center of mass energy of 7 TeV, had accumulated an integrated luminosity of about  $5 \text{ fb}^{-1}$  from both the ATLAS and CMS experiments [1]. Since April 5, 2012, the LHC has been running at an 8 TeV collision energy, and has collected about  $12 \text{ fb}^{-1}$  of data in each detector by August 20. The LHC, running in this “LHC-8” mode, is expected to produce up to about  $20 - 30 \text{ fb}^{-1}$  of data apiece in the ATLAS and CMS detectors by the end of this year, which will amount to  $40 - 60 \text{ fb}^{-1}$  in total. This will enable the LHC to make incisive tests of the predictions of many competing models of the origin of electroweak symmetry breaking (EWSB), from the Standard Model (SM) with a single Higgs boson, to models with multiple Higgs bosons, and to so-called Higgsless models of the EWSB. The Higgsless models [2, 3] contain new spin-1 gauge bosons which play a key role in EWSB by delaying unitarity violation of longitudinal weak boson scattering up to a higher ultraviolet (UV) scale [4] without invoking a fundamental Higgs scalar. Very recently, the effective UV completion of the minimal three-site Higgsless model

[5] was presented and studied in [6] which showed that the latest LHC signals of a Higgs-like state with mass around  $125 - 126$  GeV [7] can be readily explained, in addition to the signals of new spin-1 gauge bosons studied in the present paper.

In this work, we explore the physics potential of the LHC-8 to discover a relatively light fermiophobic electroweak gauge boson  $W_1$  with mass  $250 - 400$  GeV, as predicted by the minimal three-site moose model [5] and its UV completion [6]. Being fermiophobic or nearly so, the  $W_1$  state is allowed to be fairly light. More specifically, the 5d models that incorporate ideally [8] delocalized fermions [9, 10], in which the ordinary fermions propagate appropriately in the compactified extra dimension (or in deconstructed language, derive their weak properties from more than one  $SU(2)$  group in the extended electroweak sector [11, 12]), yield phenomenologically acceptable values for all  $Z$ -pole observables [5]. In this case, the leading deviations from the SM appear in multi-gauge-boson couplings, rather than the oblique parameters  $S$  and  $T$ . Ref. [13] demonstrates that the LEP-II constraints on the strength of the coupling of the  $Z_0$ - $W_0$ - $W_0$  vertex allow a  $W_1$  mass as light as 250 GeV, where  $W_0$  and  $Z_0$  refer to the usual electroweak gauge bosons.

In the next section we introduce the model. Section 3 presents our analysis of the  $pp \rightarrow W_1 Z_0 \rightarrow W_0 Z_0 Z_0 \rightarrow jj\ell^+\ell^-\ell^+\ell^-$  process at the LHC-8. Finally, we demonstrate that the LHC-8 should be able to sensitively probe  $W_1$  bosons in the mass-range of  $250 - 400$  GeV by the end of this year.

## II. 2. THE MODEL

We study the minimal deconstructed moose model at LHC-8 in a limit where its gauge sector is equivalent to the “three site model” [5] or its UV completed “minimal linear moose model” (MLMM) [6] whose gauge boson phenomenology was previously studied [14][15] for the 14 TeV LHC. Both the three site model and the MLMM are based on the gauge group  $SU(2)_0 \otimes SU(2)_1 \otimes U(1)_2$ , as depicted by Fig.1 and its gauge sector is the same as that of the BESS models [16, 17] or the hidden local symmetry model [18–22]. The extended electroweak symmetry spontaneously breaks to electromagnetism when the distinct Higgs link-fields  $\Phi_1$  connecting  $SU(2)_0$  to  $SU(2)_1$  and  $\Phi_2$  connecting  $SU(2)_1$  to  $U(1)_2$  acquire vacuum expectation values (VEVs)  $f_{1,2}$ . The weak scale  $v \simeq 246$  GeV is related to those VEVs via  $v^{-2} = f_1^{-2} + f_2^{-2}$  and, for illustration, we take  $f_1 = f_2 = \sqrt{2}v$ . Below the symmetry breaking scale, the gauge boson spectrum includes an extra set of weak bosons ( $W_1, Z_1$ ), in addition to the standard-model-like weak bosons ( $W_0, Z_0$ ) and the photon. Furthermore, the scalar sector of the MLMM [6] contains two neutral physical Higgs bosons ( $h^0, H^0$ ), as well as the six would-be Goldstones eaten by the corresponding gauge bosons

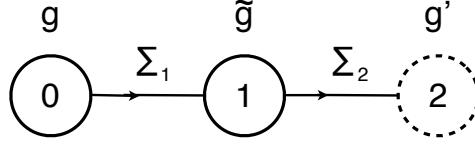


FIG. 1: Moose diagram of the minimal linear moose model (MLMM) with the gauge structure  $SU(2)_0 \times SU(2)_1 \times U(1)_2$  as well as two independent link fields for spontaneous symmetry breaking. The relevant parameter space of phenomenological interest is where the gauge couplings obey  $g, g' \ll \tilde{g}$ .

$(W_0, Z_0)$  and  $(W_1, Z_1)$ .

In our previous work [14] on the phenomenology of such spin-1 new gauge bosons at a 14 TeV LHC, we studied the potential for detecting the  $W_1$  via both the weak boson fusion  $pp \rightarrow W_0 Z_0 jj \rightarrow W_1 jj \rightarrow W_0 Z_0 jj$  and the associated production process  $pp \rightarrow W_1 Z_0 \rightarrow W_0 Z_0 Z_0$ . Focusing on the mass range 400 – 1000 GeV, we found that associated production would require less integrated luminosity than the gauge boson fusion channel at the lower end of that mass range, as shown in Fig. 4 of Ref. [14]. Extrapolating that result to lower  $W_1$  masses and a lower LHC collision energy, we have found in this work that for the LHC-8, the best process for detecting  $W_1$  in the mass range 250 – 400 GeV is also the associated production,  $pp \rightarrow W_1 Z_0 \rightarrow W_0 Z_0 Z_0 \rightarrow jj \ell^+ \ell^- \ell^+ \ell^-$ , where we select the  $W_0$  decays into dijets and the  $Z_0$  decays into electron or muon pairs.

One distinctive feature of the MLMM is that the unitarity of high-energy longitudinal weak boson scattering is maintained jointly by the exchange of both the new spin-1 weak bosons and the spin-0 Higgs bosons [6]. This differs from either the SM (in which unitarity of longitudinal weak boson scattering is ensured by the exchange of the Higgs boson alone) [23] or the conventional Higgsless models (in which unitarity of longitudinal weak boson scattering is ensured by the exchange of spin-1 new gauge bosons alone) [4]. It has been shown [13] that the scattering amplitudes in such highly deconstructed models with only three sites can accurately reproduce many aspects of the low-energy behavior of 5d continuum theories.

The original Lagrangian of the three site model was given in a nonlinear Higgsless form [5],

$$\mathcal{L}_{\text{HL}} = \frac{1}{4} \text{Tr} \left[ f_1^2 (D_\mu \Sigma_1)^\dagger (D^\mu \Sigma_1) + f_2^2 (D_\mu \Sigma_2)^\dagger (D^\mu \Sigma_2) \right], \quad (1)$$

where the nonlinear sigma fields  $\Sigma_j = \exp[i\pi_j^a \tau^a / f_j]$  and  $\tau^a$  denotes the Pauli matrices. The gauge

covariant derivatives take the following forms,

$$D^\mu \Sigma_1 = \partial^\mu \Sigma_1 + ig W_L^{a\mu} \frac{\tau^a}{2} \Sigma_1 - i\tilde{g} \Sigma_1 W_H^{a\mu} \frac{\tau^a}{2}, \quad (2a)$$

$$D^\mu \Sigma_2 = \partial^\mu \Sigma_2 + i\tilde{g} W_H^{a\mu} \frac{\tau^a}{2} \Sigma_2 - ig' \Sigma_2 W_R^{3\mu} \frac{\tau^3}{2}. \quad (2b)$$

Extending this construction, we will include the radial Higgs excitations in the sigma fields. We introduce the two radial Higgs excitations  $h_j$  as follows,

$$\Phi_j = (f_j + h_j) \Sigma_j, \quad \Sigma_j = \exp[i\pi_j^a \tau^a / f_j], \quad (3)$$

where the Higgs fields  $\Phi_j$  are  $2 \times 2$  matrices, and the Higgs bosons  $h_{1,2}$  are gauge-singlets. Thus, we can write down the Lagrangian of the MLMM by including the radial Higgs excitations for (1),

$$\mathcal{L} = \frac{1}{4} \text{Tr} \left[ (D_\mu \Phi_1)^\dagger (D^\mu \Phi_1) + (D_\mu \Phi_2)^\dagger (D^\mu \Phi_2) \right] - V(\Phi_1, \Phi_2), \quad (4)$$

where  $V(\Phi_1, \Phi_2)$  denotes the scalar potential as given in [6], but is not needed for the current study. In the unitary gauge, this Lagrangian is identical to the renormalizable MLMM studied in [6]. Since our current phenomenological study (next section) just focuses on the detection of spin-1 new gauge bosons in the MLMM, the radial Higgs excitations included in the Lagrangian (4) do not affect our collider analysis. For the following LHC analyses, we will always take  $f_1 = f_2 = \sqrt{2}v$ .

The unitarity of the generic longitudinal scattering amplitude of  $W_0^L W_0^L \rightarrow W_0^L W_0^L$ , in the presence of any numbers of spin-1 new gauge bosons  $V_k (= W_k, Z_k)$  and spin-0 Higgs bosons  $h_k$ , was recently studied in Ref. [6]. It has been shown that requiring the exact cancellation of the asymptotic  $E^2$  terms<sup>1</sup> in the scattering amplitude imposes the following sum rule on the couplings and masses [6],

$$G_{4W_0} - \frac{3M_{Z_0}^2}{4M_{W_0}^2} G_{W_0 W_0 Z_0}^2 = \sum_k \frac{3M_{Z_k}^2}{4M_{W_0}^2} G_{W_0 W_0 Z_k}^2 + \sum_k \frac{G_{W_0 W_0 h_k}^2}{4M_{W_0}^2}. \quad (5)$$

Here  $G_{V_i V_j V_k}$  is the cubic coupling among the three vector bosons indicated,  $Z_k$  is the  $k$ th Kaluza-Klein mode of the  $Z$  boson, and  $G_{4W_0}$  is the quartic coupling of  $W_0$  bosons. Eq. (5) extends the corresponding Higgsless sum rule derived in [24]. For the current MLMM, the general sum rule (5) becomes [6],

$$G_{4W_0} - \frac{3M_{Z_0}^2}{4M_{W_0}^2} G_{W_0 W_0 Z_0}^2 = \frac{3M_{Z_1}^2}{4M_{W_0}^2} G_{W_0 W_0 Z_1}^2 + \frac{G_{W_0 W_0 h}^2 + G_{W_0 W_0 H}^2}{4M_{W_0}^2}, \quad (6)$$

---

<sup>1</sup> Here  $E$  denotes the center-of-mass energy of the relevant scattering process.

where the symbols ( $h, H$ ) denote the two mass-eigenstate Higgs bosons, and we have  $G_{W_0 W_0 h_1}^2 + G_{W_0 W_0 h_2}^2 = G_{W_0 W_0 h}^2 + G_{W_0 W_0 H}^2$ . Because there is only a single extra set of weak gauge bosons in this theory, the sum over KK modes on the right-hand-side of (5) reduces to a single term. Then, with the Lagrangian (4) of the MLMM, we have explicitly verified the sum rule (6). Hence, the unitarity of the longitudinal weak boson scattering in the MLMM is ensured jointly [6] by exchanging both the new spin-1 weak bosons  $W_1/Z_1$  and the spin-0 Higgs bosons  $h/H$ . We also note that the  $hWW$  and  $hZZ$  couplings are generally suppressed [6] relative to the SM values because of the VEV ratio  $f_2/f_1 = O(1)$  and the  $h - H$  mixing. As shown in [6], the MLMM can predict an enhanced diphoton rate for the light Higgs boson  $h$  with mass  $125 - 126$  GeV via gluon fusions, while the Higgs signals via the associate production  $q\bar{q}' \rightarrow hV_0$  and vector boson fusion  $q\bar{q}' \rightarrow hq_3q_4$  (with  $h \rightarrow b\bar{b}, \tau\bar{\tau}$ ) are always lower than the SM.

### III. 3. ANALYSIS OF $W_1^\pm$ DETECTION AT THE LHC-8

In this section, we study the partonic-level signals and backgrounds for detecting  $W_1^\pm$  states at the LHC-8 in the associated production channel. The signal events proceed via the process  $pp \rightarrow W_1 Z_0 \rightarrow W_0 Z_0 Z_0 \rightarrow jj\ell^+\ell^-\ell^+\ell^-$  where the leptons can be either electrons or muons. We have systematically computed all the major SM backgrounds for the  $jj4\ell$  final state, including the irreducible backgrounds  $pp \rightarrow W_0 Z_0 Z_0 \rightarrow jj4\ell$  ( $jj = q\bar{q}'$ ) without the contribution of  $W_1$ , as well as the reducible backgrounds  $pp \rightarrow ggZ_0 Z_0 \rightarrow jj4\ell$ ,  $pp \rightarrow Z_0 Z_0 Z_0 \rightarrow jj4\ell$ , and the SM  $pp \rightarrow jj4\ell$  other than the above reducible backgrounds.

We performed the parton level calculations at tree-level using two different methods and two different gauges to check the consistency. In one calculation, we used the helicity amplitude approach [27] to generate the signal and backgrounds. We also calculated both the signal and background using CalcHEP [30, 31]. For the signal calculation in CalcHEP, we used FeynRules [25] to implement the minimal Higgsless model [26]. We found satisfactory agreement between these two approaches and between both unitary and 't Hooft-Feynman gauge. We used a scale of  $\sqrt{\hat{s}}$  for the strong coupling in the backgrounds and  $\sqrt{\hat{s}}/2$  for the CTEQ6L [28] parton distribution functions. We included both the first and second generation quarks in the protons and jets, and both electrons and muons in the final-state leptons.

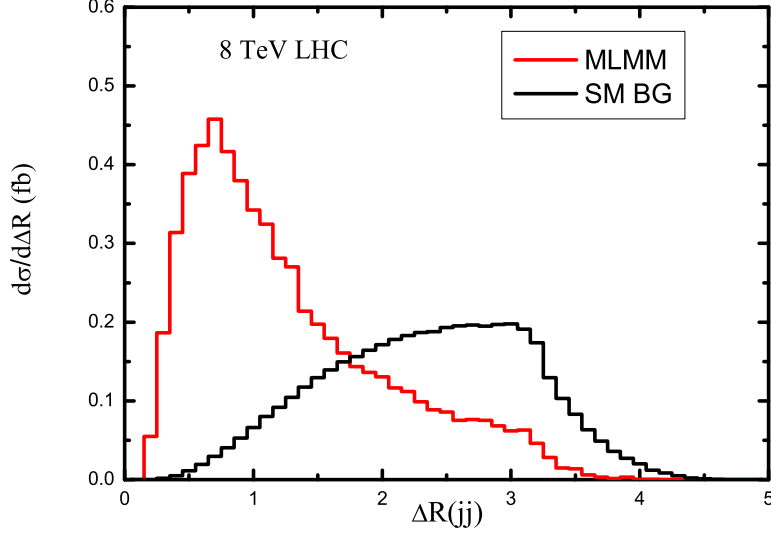


FIG. 2: Event distribution  $\Delta R(jj)$  at LHC-8, for the MLMM with  $M_{W_1} = 300$  GeV (red curve), and for the SM backgrounds (black curve) which peak around the large  $\Delta R(jj)$ .

In our calculations, we impose basic acceptance cuts,

$$\begin{aligned} p_{T\ell} &> 10 \text{ GeV}, & |\eta_\ell| &< 2.5, \\ p_{Tj} &> 15 \text{ GeV}, & |\eta_j| &< 4.5, \end{aligned} \quad (7)$$

and also a reconstruction cut for identifying  $W_0$  bosons that decay to dijets,

$$M_{jj} = 80 \pm 15 \text{ GeV}. \quad (8)$$

The same cuts were imposed for our previous analysis for the 14 TeV LHC [14], where we found that a minimum separation cut on the two jets was not necessary. We find that these cuts are also effective for  $W_1^\pm$  searches at the LHC-8.

We further analyze the distributions of the dijet opening-angle  $\Delta R(jj)$  in the decays of  $W_0 \rightarrow jj$  for both the signal and SM background events. This is depicted in Fig. 2. We find that the signal events are peaked in the small opening-angle region around  $\Delta R(jj) \sim 0.6$ , while the SM backgrounds tend to populate the range of larger opening angles, with a broad bump around  $\Delta R(jj) = 1.5 - 3.3$ . In order to sufficiently suppress the SM backgrounds, we find the following opening-angle cut<sup>2</sup> to be very effective [29],

$$\Delta R(jj) < 1.6. \quad (9)$$

<sup>2</sup> These are somewhat weaker than the cut of  $\Delta R(jj) < 1.5$  imposed in [14].

At the LHC-8, we note that the above cut reduces the signal events by only 10 – 15%, but removes about 72 – 80% of the SM backgrounds.

Next, we present the invariant-mass distribution  $M(Z_0 jj)$  in Fig. 3, where we compare the signal with all relevant SM backgrounds. We have used  $M_{W_1} = 300$  GeV as a sample value for a relatively light  $W_1$  boson. Because the two  $Z^0$  bosons are indistinguishable, each event is included twice, i.e., at the two  $M(Z_0 jj)$  values corresponding to combining each  $Z_0$  boson with the dijets. The predicted signal events (plus SM backgrounds and the signal-derived combinatorial background) are shown for the MLMM (red curve). We have systematically computed all the major SM backgrounds for the  $jj4\ell$  final state, including the irreducible backgrounds  $pp \rightarrow W_0 Z_0 Z_0 \rightarrow jj4\ell$  ( $jj = qq'$ ) without the contribution of  $W_1$ , as well as the reducible backgrounds  $pp \rightarrow qg Z_0 Z_0 \rightarrow jj4\ell$  (purple curve, 2nd from bottom),  $pp \rightarrow gg Z_0 Z_0 \rightarrow jj4\ell$  (green curve, bottom),  $pp \rightarrow Z_0 Z_0 Z_0 \rightarrow jj4\ell$  and other SM processes of the form  $pp \rightarrow jj4\ell$ . The summed total SM backgrounds are shown as the black curve (3rd from bottom) in Fig. 3. The irreducible background and the reducible backgrounds from  $pp \rightarrow Z_0 Z_0 Z_0 \rightarrow jj4\ell$  and other SM  $pp \rightarrow jj4\ell$  processes are so small that they are invisible in Fig. 3. We also note that the process  $pp \rightarrow W_0^* \rightarrow W_0 h^* \rightarrow W_0 Z_0 Z_0 \rightarrow jj4\ell$  is highly suppressed after all the cuts including (10) below, and is fully negligible in this analysis. From Fig. 3, we see that at LHC-8, the  $W_1$  resonance peak is distinct and the SM backgrounds are effectively suppressed.

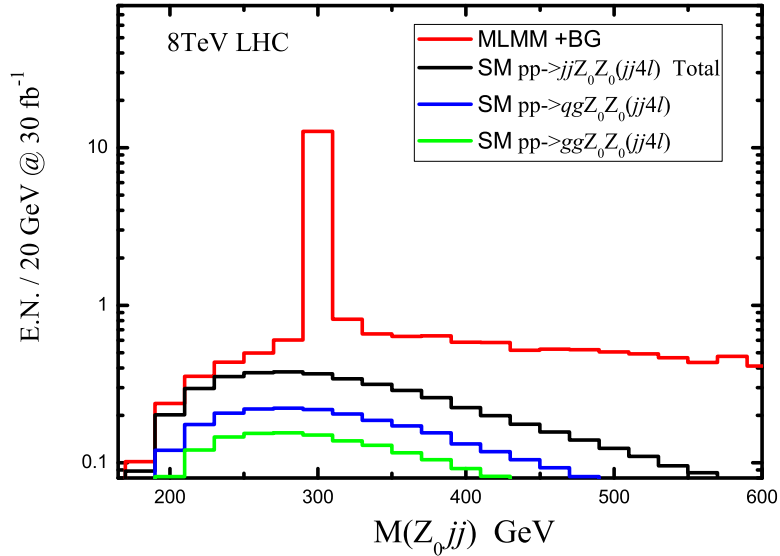


FIG. 3: Invariant-mass distribution of  $M(Z_0 jj)$  for the predicted signals of the  $W_1^\pm$  bosons with mass  $M_{W_1} = 300$  GeV and after all relevant cuts. The key of this plot identifies all curves in the order from top to bottom.



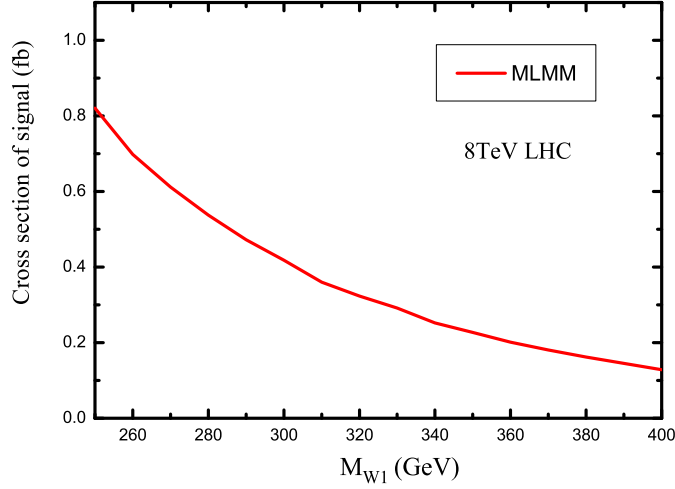


FIG. 4: Predicted signal cross section for  $pp \rightarrow W_1 Z_0 \rightarrow W_0 Z_0 Z_0 \rightarrow jj4\ell$  as a function of the  $W_1$  mass in the MLMM after all cuts at the LHC-8.

TABLE I: Predicted signal cross sections of the MLMM and the SM backgrounds for  $W_1^\pm$  production via  $pp \rightarrow W_1 Z_0 \rightarrow W_0 Z_0 Z_0 \rightarrow jj4\ell$  at the LHC-8, including all cuts described in the text.

$M_{W_1}$ (GeV)		250	300	350	400
Signal Cross Section (fb)		0.8205	0.4180	0.2271	0.1282
Background Cross Sections (fb)	$pp \rightarrow qg Z_0 Z_0$	0.0145	0.0141	0.0114	0.0083
	$pp \rightarrow gg Z_0 Z_0$	0.0101	0.0096	0.0078	0.0058
	Total	0.0246	0.0236	0.0191	0.0141

In Fig. 4, we display the predicted total signal cross section for the process  $pp \rightarrow W_0 Z_0 Z_0 \rightarrow jj4\ell$  after all cuts at the LHC-8 have been imposed; this is shown as a function of the  $W_1$  mass for the range 250 – 400 GeV. Here, we define the signal region to include all events satisfying

$$M(Z_0 jj) = M_{W_1} \pm 20 \text{ GeV}. \quad (10)$$

The cross sections of signals and backgrounds are also listed in Table I for four sample values of  $W_1$  masses,  $M_{W_1} = 250, 300, 350, 400$  GeV.

#### IV. 4. RESULTS AND CONCLUSIONS

Finally, we present the LHC-8 discovery reach for the the relatively light  $W_1$  mass-range of 250–400 GeV. To calculate the statistical significance, we use the Poisson probability which governs the random generation of uncorrelated events. If the number of events expected in the background is  $\nu$ , then the probability  $P_P(n, \nu)$  that the number of events measured will fluctuate up to  $n$  is given by

$$P_P(n, \nu) = \frac{\nu^n e^{-\nu}}{n!}. \quad (11)$$

The probability that the background will fluctuate up to the background plus the signal or higher is then given by

$$P_P(n \geq \nu + s, \nu) = \sum_{n=\nu+s}^{\infty} \frac{\nu^n e^{-\nu}}{n!}. \quad (12)$$

For this to correspond to a  $3\sigma$  or  $5\sigma$  significance, this probability must be the same as the probability for a Gaussian to fluctuate up 3 or 5 standard deviations, respectively,  $P_G(3\sigma) = 0.00135$  or  $P_G(5\sigma) = 2.87 \times 10^{-7}$  [32].

In Fig. 5, we display the required integrated luminosities for detecting the  $W_1^\pm$  signal at the  $3\sigma$  and  $5\sigma$  levels as a function of the  $W_1^\pm$  mass  $M_{W_1}$ . Table II summarizes the  $5\sigma$  reach in  $M_{W_1}$  for some sample values of the integrated luminosity at the LHC-8. In this analysis, we have included statistical errors in determining the  $W_1^\pm$  discovery potential. We anticipate that experimental analyses will include more complete detector level simulations, systematic errors and the details of detector geometry.

Fig. 5 and Table II demonstrate that the LHC-8 should be able to probe the light mass range for the  $W_1^\pm$  gauge bosons quite effectively in the minimal linear moose model studied here. In fact, it has good potential for detecting  $W_1^\pm$  with a mass below 400 GeV by the end of 2012. This is complementary to the discovery reach for heavier  $W_1^\pm$  bosons (400 GeV – 1 TeV) that our previous study [14] showed to be feasible for the LHC when running at 14 TeV collision energy.

In summary, the LHC-8 is continuing to test the origin of electroweak symmetry breaking. The minimally extended electroweak gauge structure of  $SU(2)^2 \otimes U(1)$  generically predicts the extra spin-1 gauge bosons as the unambiguous new physics beyond the SM, which give distinct new signatures at the LHC. We have demonstrated that after each of the ATLAS and CMS detectors collects up to  $20 - 30 \text{ fb}^{-1}$  of data by the end of this year, the LHC-8 should have good potential to probe the dynamics of the extended gauge symmetry breaking  $SU(2)^2 \otimes U(1) \rightarrow U(1)_{\text{em}}$ . We

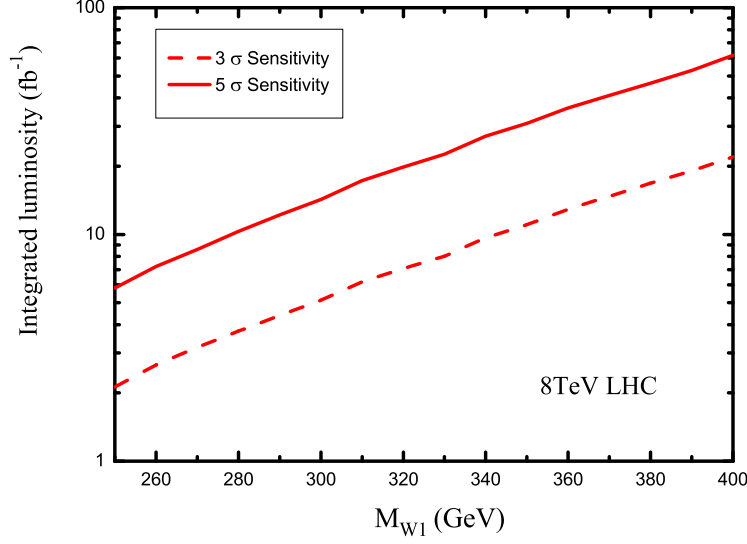


FIG. 5: Integrated luminosities required for detection of new  $W_1^\pm$  gauge bosons at the  $3\sigma$  level in the MLMM (red dashed curve), and at the  $5\sigma$  level (red solid curve) as a function of the  $W_1$  mass, at the LHC-8.

TABLE II: The  $5\sigma$  discovery reaches of the  $W_1^\pm$  bosons at the LHC-8, with the integrated luminosities  $\int \mathcal{L} = 10, 15, 20, 25, 30, 35, 40, 50, 60 \text{ fb}^{-1}$ , respectively.

$\int \mathcal{L} \text{ (fb}^{-1}\text{)}$	10	15	20	25	30	35	40	50	60
$M_{W_1} \text{ (GeV)}$	277	302	320	335	346	357	367	385	397

look forward to seeing the results.

## Acknowledgments

This research was supported by the NSF of China (grants 10625522, 10635030, 11135003, 11075086) and the National Basic Research Program of China (grant 2010CB833000); by the U.S. NSF under Grants PHY-0854889 and PHY-0705682; and by the University of Pittsburgh Particle Physics, Astrophysics, and Cosmology Center. HJH thanks CERN Theory Division for hospitality.

- 
- [1] G. Aad *et al.*, (ATLAS Collaboration), Phys. Lett. B **710**, 49 (2012) [arXiv:1202.1408 [hep-ex]]; S. Chatrchyan *et al.* (CMS Collaboration), Phys. Lett. B **710**, 26 (2012) [arXiv:1202.1488 [hep-ex]].
  - [2] C. Csaki, C. Grojean, H. Murayama, L. Pilo and J. Terning, Phys. Rev. D **69**, 055006 (2004) [hep-

- ph/0305237].
- [3] C. Csaki, C. Grojean, L. Pilo and J. Terning, Phys. Rev. Lett. **92**, 101802 (2004) [hep-ph/0308038].
  - [4] R. S. Chivukula, D. A. Dicus, H. J. He, Phys. Lett. B **525**, 175 (2002); R. S. Chivukula and H. J. He, Phys. Lett. B **532**, 121 (2002); R. S. Chivukula, D. A. Dicus, H. J. He, S. Nandi, Phys. Lett. B **562**, 109 (2003); H. J. He, Int. J. Mod. Phys. A **20**, 3362 (2005); R. S. Chivukula, H. J. He, M. Kurachi, E. H. Simmons, M. Tanabashi, Phys. Rev. D **78**, 095003 (2008).
  - [5] R. S. Chivukula, B. Coleppa, S. Di Chiara, E. H. Simmons, H. J. He, M. Kurachi, M. Tanabashi, Phys. Rev. D **74**, 075011 (2006) [arXiv:hep-ph/0607124].
  - [6] T. Abe, N. Chen, H. J. He, arXiv:1207.4103 [hep-ph].
  - [7] G. Aad *et al.*, (ATLAS Collaboration), arXiv:1207.7214 [hep-ex]; S. Chatrchyan *et al.*, (CMS Collaboration), arXiv:1207.7235 [hep-ex].
  - [8] R. S. Chivukula, E. H. Simmons, H. J. He, M. Kurachi and M. Tanabashi, Phys. Rev. D **72**, 015008 (2005) [arXiv:hep-ph/0504114].
  - [9] G. Cacciapaglia, C. Csaki, C. Grojean and J. Terning, Phys. Rev. D **71**, 035015 (2005) [arXiv:hep-ph/0409126].
  - [10] R. Foadi, S. Gopalakrishna and C. Schmidt, Phys. Lett. B **606**, 157 (2005) [arXiv:hep-ph/0409266].
  - [11] R. S. Chivukula, E. H. Simmons, H. J. He, M. Kurachi and M. Tanabashi, Phys. Rev. D **71**, 115001 (2005) [arXiv:hep-ph/0502162].
  - [12] R. Casalbuoni, S. De Curtis, D. Dolce and D. Dominici, Phys. Rev. D **71**, 075015 (2005) [arXiv:hep-ph/0502209].
  - [13] A. Belyaev, R. S. Chivukula, N. D. Christensen, H. J. He, M. Kurachi, E. H. Simmons, M. Tanabashi, Phys. Rev. D **80**, 055022 (2009) [arXiv:0907.2662]; and presentation in the Proceedings of International Workshop on “Strong Coupling Gauge Theories in LHC Era” (SCGT-2009), arXiv:1003.1786 [hep-ph].
  - [14] H. J. He, Y. P. Kuang, Y. Qi, B. Zhang, A. Belyaev, R. S. Chivukula, N. D. Christensen, A. Pukhov, E. H. Simmons, Phys. Rev. D **78**, 031701 (2008) [arXiv:0708.2588].
  - [15] T. Ohl and C. Speckner, Phys. Rev. D **78** (2008) 095008 [arXiv:0809.0023]; T. Abe, T. Masubuchi, S. Asai, and J. Tanaka, Phys. Rev. D **84** (2011) 055005 [arXiv:1103.3579]; F. Bach and T. Ohl, Phys. Rev. D **85** (2012) 015002 [arXiv:1111.1551].
  - [16] R. Casalbuoni, S. De Curtis, D. Dominici and R. Gatto, Phys. Lett. B **155**, 95 (1985).
  - [17] R. Casalbuoni *et. al.*, Phys. Rev. **D53**, 5201 (1996) [hep-ph/9510431].
  - [18] M. Bando, T. Kugo, S. Uehara, K. Yamawaki and T. Yanagida, Phys. Rev. Lett. **54**, 1215 (1985).
  - [19] M. Bando, T. Kugo and K. Yamawaki, Nucl. Phys. B **259**, 493 (1985).
  - [20] M. Bando, T. Fujiwara, and K. Yamawaki, Prog. Theor. Phys. **79**, 1140 (1988).
  - [21] M. Bando, T. Kugo, and K. Yamawaki, Phys. Rept. **164**, 217 (1988).
  - [22] M. Harada and K. Yamawaki, Phys. Rept. **381**, 1 (2003) [hep-ph/0302103].
  - [23] J. M. Cornwall, D. N. Levin, and G. Tiktopoulos, Phys. Rev. Lett. **30** (1973) 1268; Phys. Rev. D **10** (1974) 1145; C. H. Llewellyn Smith, Phys. Lett. **46B** (1973) 233. D. A. Dicus and V. S. Mathur, Phys.

- Rev. D **7** (1973) 3111; B. W. Lee, C. Quigg, and H. B. Thacker, Phys. Rev. Lett. **38** (1977) 883; Phys. Rev. D **16** (1977) 1519; M. S. Chanowitz and M. K. Gaillard, Nucl. Phys. B **261** (1985) 379.
- [24] R. S. Chivukula, H. J. He, M. Kurachi, E. H. Simmons, M. Tanabashi, Phys. Rev. D **78**, 095003 (2008) [arXiv:0808.1682].
- [25] N. D. Christensen and C. Duhr, Comput. Phys. Commun. **180**, 1614 (2009) [arXiv:0806.4194 [hep-ph]].
- [26] N. D. Christensen, P. de Aquino, C. Degrande, C. Duhr, B. Fuks, M. Herquet, F. Maltoni and S. Schumann, Eur. Phys. J. C **71**, 1541 (2011) [arXiv:0906.2474 [hep-ph]].
- [27] K. Hagiwara and D. Zeppenfeld, DESY-85-133; K. Hagiwara, R. D. Peccei, D. Zeppenfeld and K. Hikasa, DESY-86-058 (1986); K. Hagiwara and D. Zeppenfeld, KEK Preprint 87-158 (1988).
- [28] J. Pumplin, D. R. Stump, J. Huston, H. L. Lai, P. Nadolsky, W. K. Tung, JHEP **07**, 012 (2002).
- [29] This kind of cut should be applied to separated jets. Experimentally, two jets are separable if  $\Delta R_{jj} > 0.5$  [see for instance, S. Ask (ATLAS Collaboration), arXiv:1106.2061], and two jet-cones do not overlap at all if  $\Delta R_{jj} > 1$ . So the cut (9) can be realized.
- [30] A. Pukhov, E. Boos, M. Dubinin, V. Edneral, V. Ilyin, D. Kovalenko, A. Kryukov and V. Savrin, *et al.*, hep-ph/9908288.
- [31] A. Pukhov, hep-ph/0412191.
- [32] K. Nakamura *et al.*, [Particle Data Group], J. Phys. G **37**, 075021 (2010) [No. 7A].